The Effect of Compatibilizer on the Co-Continuity and Nanoclay Dispersion Level of TPE Nanocomposites Based on PP/EPDM

Amin Mirzadeh,[1] Pierre G. Lafleur,[1] Musa R. Kamal,[2] Charles Dubois[1]
[1] *Chemical Engineering Department, Ecole Polytechnique, Montreal, Quebec, Canada H3C 3A7*

[2] *Chemical Engineering Department, McGill University, Montreal, Quebec, Canada H3A 2B2*

The effects of different polypropylene (PP)-g-maleic anhydride polymers, used as compatibilizers, on the degree of exfoliation and co-continuity of PP/ethylene-propylene-diene terpolymer (EPDM) thermoplastic elastomer (TPE)/clay nanocomposites were investigated. X-ray diffraction and transmission electron microscopic micrographs showed that nanocomposites ranged from intercalated structure to a coexistence of intercalated tactoids and exfoliated layers. The observed significant increase in crystallization temperature (~20°C) could be beneficial for molding applications, because it means faster solidification and shorter cycle time. The rheological characteristic relaxation time of the compatibilizer correlated with the dispersion level in the nanocomposites. Solvent extraction and gravimetry measurements of continuity showed that compatibilizer affects the co-continuity composition range through its effect on the dispersion level of nanoclays. At high EPDM concentration, the continuity of the thermoplastic phase for semi-exfoliated TPE nanocomposites was higher than in the corresponding TPEs. Considering that TPE formation is the first step for thermoplastic vulcanizate production, where the thermoplastic phase should have a certain level of continuity, these results suggest that higher levels of EPDM could be incorporated into the semi-exfoliated system before losing matrix continuity. It was also observed that there is a direct relation between the magnitude of the normalized stress growth viscosity overshoot and the continuity of TPE nanocomposites. **POLYM. ENG. SCI., 50:2131–2142, 2010.** **© 2010 Society of Plastics Engineers**

INTRODUCTION

Polypropylene (PP) layered silicate nanocomposites have received much attention due to their high performance [1–3]. The use of a compatibilizer has made it easier to produce such nanocomposites by melt intercalation [4–8]. Maleic anhydride-grafted PP (PP-g-MA) has been used extensively as a compatibilizers in the preparation of PP/clay nanocomposites, with significant improvements in structure and mechanical properties. However, there is still need to identify one or more compatibilizer properties that could serve as good predictor(s) of the compatibilizer effectiveness. For example, studies showed that intercalation of the polymer did not occur, when the content of MA in the PP-g-MA polymer was low (acid value = 7 mg KOH/g for Mw = 12,000) [3, 7]. It was also shown that intercalation was enhanced, when the PP-g-MA content was increased until it reached an intermediate level (acid value = 26 mg KOH/g, Mw = 40,000). Further increase in the acid value (e.g., acid value = 52 mg KOH/g) had no further influence on the increase of d-spacing of the layered silicate. The evaluation of the effects of three levels of molecular weight (low, medium, and high) of PP-g-MA on the morphology and the mechanical properties of PP nanocomposites revealed that the nanocomposites incorporating the highest PP-g-MA molecular weight (Mw = 330,000, MA = 0.5 wt%) yielded the best overall mechanical properties [9]. In another study, it was reported that the degree of the intercalation and the uniformity of clay dispersion were affected by both molecular weight and the MA content [10]. The present work investigates the effects of different PP-g-MA compatibilizers on the degree of exfoliation and co-continuity of thermoplastic elastomer (TPE) nanocomposites based on PP/ethylene-propylene-diene terpolymer (EPDM). According to the classical point of view, an ideally co-continuous structure is defined as the coexistence of at least two continuous structures within the same volume. This implies that three-dimensional spatial continuity, at some finite scale of mixing, could be found for both components [11]. Other definitions to describe co-continuous structures refer to structures with dual-phase continuity, co-phase continuity, interpenetrating

Correspondence to: Musa R. Kamal; e-mail: musa.kamal@mcgill.ca
Contract grant sponsor: Natural Sciences and Engineering Research Council of Canada.
DOI 10.1002/pen.21744
Published online in Wiley Online Library (wileyonlinelibrary.com).

polymer networks (IPNs), IPNs of phases, interpenetrating co-continuous phase structure or interpenetrating polymer blends [11–14]. Lyngaae-Jorgensen et al. [15] suggested a definition based on the percolation threshold theory that considers different structure types allowing some part of the components to be present in separate domains that are not part of the network structure. Therefore, a co-continuous structure is described as one wherein at least a part of each phase forms a coherent continuous structure permeating the whole volume [11]. Thus, as the amount of the minor component in the blend is increased, the percolation structure is reached, suggesting a fully co-continuous structure. The percolation-based definition has been used in the present study to determine the continuity index. Thus, the continuity index, continuity fraction or the degree of (co-continuity) is defined as the fraction of a component that is part of the percolating structure [11, 12, 15]. The classical and percolation definitions become equivalent when the continuity index is equal to one for both phases.

One of the important mechanisms of droplet formation during blending involves the breakup of highly elongated threads via capillary instabilities, leading to a sequence of adjacent smaller droplets. The breakup occurs after the thread diameter reaches a size for which the capillary number, Ca, becomes <1, and if the residence time during the mixing process is longer than the break-up time [11]. The break-up time, t_b, is given by:

$$t_b = \left(\frac{\eta_m B}{\Omega(1,\lambda)\sigma}\right) \ln\left(\frac{0.8B}{2\alpha_0}\right), \quad (1)$$

where α_0 is the amplitude of the initial distortion, and $\Omega(l,\lambda)$ is the Tomokita function which is a dimensionless distortion growth rate, depending on the distortion wavelength (l) and the viscosity ratio (λ). The diameter of the elongated thread B depends on the total amount of strain, as follows: (*Eq. 2*).

$$B = 2R_0(1+\gamma^2)^{-\frac{1}{4}}, \quad (2)$$

where γ is strain and R_0 is the starting radius of a spherical particle. The above suggests that the viscosity ratio, interfacial tension, and processing conditions are factors that influence co-continuity.

Bhadane et al. [16] evaluated a variety of PP/EPDM blends with viscosity ratios in the range 0.2–5.0. The blends were prepared at shear stresses of 11.7–231.4 kPa. They showed that, at low blend compositions, the dispersed phase appeared as stable fibers with small diameters in the range of 50–200 nm. Continuity was established by fiber–fiber coalescence. They also reported that a sevenfold variation in the viscosity ratio had virtually no influence on the continuity index or morphology. In fact, they obtained a single continuity master curve for PP/EPDM blends at these conditions.

Another important parameter that influences co-continuous structure is interfacial tension. The effect of interfacial tension on the co-continuity range was studied by Willemse et al. [17]. They chose different pairs of polymers having different interfacial tension values but the same viscosity ratio. They found that, in systems with higher interfacial tension, the onset volume fraction of co-continuity was higher and the co-continuity range was narrower, compared to systems with low interfacial tension. This behavior was similar for both high viscosity ratio and low viscosity ratio systems.

The present study deals with the preparation of nanocomposites based on TPE and clay. Such systems are of interest, because of their rubber-like behavior and high performance [18–21]. As nanocomposite formation usually involves the use of PP-g-MA as a compatibilizer, the molecular weight of the compatibilizer will affect the viscosity ratio and ultimately the degree of intercalation or exfoliation. Moreover, the above two parameters can affect the co-continuity composition range. The latter is quite important, because TPE formation is usually the first step of thermoplastic vulcanizates (TPV) production, and a perquisite condition for TPV formation is thermoplastic phase continuity.

EXPERIMENTAL

Materials

"Profax" 6523 (Basell Polyolefins) general purpose PP homopolymer resin, with a melt flow index (MFI) of four (g/10 min), was used as the thermoplastic phase. "Buna" EP T 6470 (LANXESS) EPDM, with ethylidene norbornene, showing a diene of 3.9–5.1% and a Mooney viscosity of 52–62 M, was used as the rubber phase. Cloisite 15A (Southern Clay Products), which is a surface modified Montmorillonite (MMT) with di-methyl, di-hydrogenated tallow ammonium chloride, was used as the nanoclay.

Four grades of PP-g-MA with different MFI values, Orevac 18729, 18732, 18750, CA 100 (Arkema), were used as compatibilizers. Functionality of PP-g-MA for all of the above compatibilizers is in the medium range. They were sorted and designated by numbers in ascending order of their MFI. Table 1 shows the information available about their properties. Irganox B 225 (Ciba) primary phenolic type was used as the antioxidant. Also, xylene and cyclohexane (Laboratoire Mat, 99% purity) were used as solvents in extraction experiments.

Blend Preparation and Nomenclature

Masterbatch Preparation. Four masterbatches (MBs) consisting of PP/PP-g-MA/Cloisite15A in the ratios (60/30/10 wt%) were prepared. Each MB contained one of the four PP-g-MA compatibilizers. The different MBs were designated MBi, where i = 1–4 refers to the corre-

 DOI 10.1002/pen

TABLE 1. Properties of compatibilizers.

Physical	18,729 (1)	18,732 (2)	CA100 (3)	18,750 (4)	Test method
Density (g/cm^3)	0.900	0.890	0.900	0.920	ISO 1183
Melt mass flow rate (g/10 min)	4.5	8.0	10	35	ISO 1133
Tensile strength @ break (MPa)	41	20	22	21	ASTM D638
Tensile elongation @ break (%)	620	500	500	500	ASTM D638
Vicat softening temperature (°C)	137	120	147	121	ISO 306
Melting point (°C)	162	134	167	160	DSC

sponding compatibilizer used in the formulation. The MBs were melt-compounded in a laboratory scale co-rotating, closely intermeshing, twin-screw extruder (Leistritz ZSE-18HP). The temperature distribution in the extruder was maintained at 185, 190, 190, 190, 195, 195, 195, and 190°C from the hopper to the die, and the screw rotation speed was fixed at 200 rpm Cloisite was fed to the extruder through the side feeder, at a location where the granules were already partially melted.

Nanocomposite Preparation. To prepare PP nanocomposites with 5 wt% of Cloisite 15A, the pellets of the MB were mixed with the PP, using the twin screw extruder. For this operation, the temperature profile in the extruder was 175, 180, 185, 190, 190, and 185°C from the hopper to the die. The screw speed was held at 600 rpm A small amount (0.5 wt%) of Irganox B 225 antioxidant was added to the mixture to reduce the oxidative degradation of PP. PP nanocomposites were designated as Nx, where x refers to the compatibilizer used in the nanocomposite.

TPE Nanocomposites Preparation. TPE nanocomposites were prepared using a Brabender (internal mixer) at 100 rpm and 200°C. The mixing volume was 30 ml. The compositions of the blends and related nomenclature are given in Table 2. TPE nanocomposites were designated as TPENx.yy, where x and yy indicate the corresponding compatibilizer and EPDM weight percent, respectively.

Characterization Steps

Thermogravimetric Analysis. Thermogravimetric analysis (TGA Q500 V6.5 Build 196, TA instruments) was performed to determine the amount of di-methyl, di-hydrogenated tallow ammonium chloride in Cloisite 15A and the level of nanoclay in MBs and nanocomposites, as well as decomposition temperatures. The samples were heated from 30°C to 600°C at a rate of 15°C/min.

Differential Scanning Calorimetry. Differential scanning calorimetry (DSC Q1000 V9.6 Build 290, TA instruments) tests were carried out to study the crystallinity and the possible nucleating effect of nanoclays. The samples were first heated from 30°C to 210°C at a rate of 10°C/min and were kept at 210°C for 5 min to erase prior thermal and mechanical history. The samples were then cooled from 210°C to 30°C at a rate of 10°C/min. The peak and onset crystallization temperatures were determined from the cooling scans. All measurements were performed in nitrogen atmosphere.

X-ray Diffraction. To evaluate the dispersion of nanoclay in the MBs, nanocomposites and TPE nanocomposites, X-ray diffraction (XRD) was carried out at room temperature using an X-ray diffractometer (Philips model X'PER) in the low angle range of 2θ. The X-ray source was Cu-K_a radiation ($\lambda = 1.540598$ Å), using a 50 kV voltage generator and a 40 mA current. The basal spacing of silicates was estimated from the position of the plane peak in the Wide Angle X-ray Diffraction (WAXD) intensity profile using Bragg's law. The angular step size was 0.005° with a step time equal to 1 s from 2° to 10° and 0.5° to 4°.

Electron Microscopy. Nanoclay dispersion in the thermoplastic phase and morphology of the TPEs were studied using scanning electron microscopy (SEM) and transmission electron microscopy (TEM). For SEM, irradiated samples were first microtomed using a glass knife under liquid nitrogen. The instrument was a Leica-Jung RM 2065 equipped with a cryochamber. Subsequently, the samples were etched with xylene vapor for 10 (s) and coated with gold–palladium alloy. SEM micrographs were obtained using a scanning electron microscope (JSM 840, Jeol) operated at a voltage of 15 kV. To calculate the number average diameter (D_n) and the volume average diameter (D_v), the SEM micrographs were analyzed using

TABLE 2. Nomenclature of TPV and TPE nanocomposites based on their compositions.

EPDM/N1 (wt%)	50/50	TPEN1.50
	60/40	TPEN1.60
	70/30	TPEN1.70
EPDM/N2 (wt%)	50/50	TPEN2.50
	60/40	TPEN2.60
	70/30	TPEN2.70
EPDM/N3 (wt%)	50/50	TPEN3.50
	60/40	TPEN3.60
	70/30	TPEN3.70
EPDM/N4 (wt%)	50/50	TPEN4.50
	60/40	TPEN4.60
	70/30	TPEN4.70

a digitizing table and user-defined transformer file [22]. To observe nanoclay dispersion, the amorphous phase of PP was removed. Further details regarding this technique have been explained elsewhere [23].

For TEM, PP nanocomposites were first trimmed to obtain a truncated pyramid section with a razor blade, to avoid the high pressure on the diamond knife. Then, they were ultra-microtomed at -130°C using a diamond knife to prepare samples with thickness of 50 nm. A water bath was used to transfer the micro-thin sections to 200-mesh copper grids. Micrographs were taken with a TEM (JEM-2100F, Jeol) and recorded with a digital camera.

Solvent Extraction and Gravimetry for Continuity. This technique was used to estimate the continuity of EPDM in TPE nanocomposite samples. Because surface area to volume ratio could affect the results, three samples of approximately $8 \times 8 \times 1.4$ mm^3 were prepared from each of the noncrosslinked blends.

The specimens were immersed in 35 ml of fresh cyclohexane solvent in a centrifuge tube for 3 days at room temperature, while they were shaken constantly. Then, the sample was dried in a vacuum oven at 60°C. This process was repeated consecutively at least three times, until the sample weight remained unchanged.

To estimate the continuity index of PP in the various systems, gamma irradiation was carried out in air with $_{27}$Co source, to fix the EPDM morphology. In this regard, TPE blends, together with the pure materials were irradiated with a dose rate of 20 kGy/h for 8 h, using commercial carrier-type 8900 irradiator. Further details regarding this technique have been described elsewhere [16, 24]. The irradiated blends were cut into the same size. These samples were immersed in 100 ml of boiling xylene for an hour and dried. The well-dried samples were subjected to the same procedure till the complete phase removal was confirmed by comparing the sample weight after consecutive drying steps. The ratio between the extracted mass of a specific phase and its total content, based on a defined cube, is the continuity index, ϕ_i, calculated as follows:

$$\phi_i = \frac{W_{1i} - W_{2i}}{W_{1i}}, \tag{3}$$

where W_{1i} and W_{2i} represent the weights of component i before and after extraction, respectively.

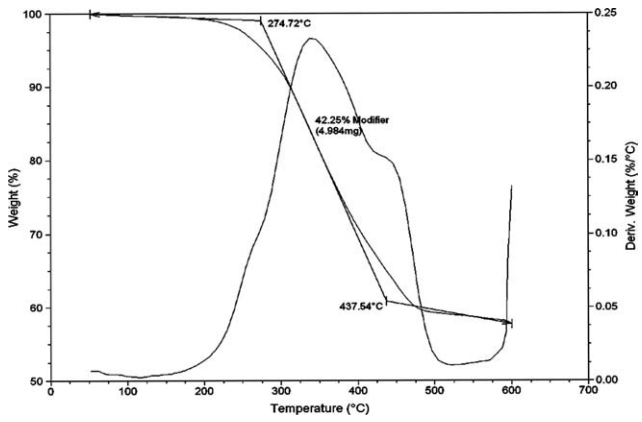

FIG. 1. Thermo-gravimetric analysis of Cloisite 15A.

TABLE 3. Nanoclay content for the masterbatches and nanocomposites obtain by TGA patterns.

	MB1	N1	MB2	N2	MB3	N3	MB4	N4
Cloisite 15A content (wt%)	10.3	4.8	10.1	4.9	9.5	4.7	9.7	4.7
STDV	2.4	0.1	0.7	0.1	1.5	0.1	0.4	0.1

Rheological Measurements. Rheological measurements were carried out using a parallel plate rheometer, ARES (Rheometrics Scientific) with 25-mm diameter parallel disc geometry at 200°C. In all cases, the linearity of the sample response with respect to stress amplitude was verified. Nitrogen gas was used to prevent thermal oxidation of the materials.

RESULTS AND DISCUSSION

Characterization of PP/Clay Nanocomposites

Thermogravimetry. TGA was used to estimate the actual amounts of Cloisite 15A in the MBs and in PP nanocomposites, and to evaluate the thermal degradation characteristics of the modifier. Figure 1 shows that the modifier started to decompose at about 240°C, which is higher than the maximum processing temperature. Since about 43 wt% of Cloisite 15A is attributable to the modifier, the average nanoclay content was calculated based on the TGA analysis of the prepared MBs (Table 3). The observed differences are reasonable, considering the use of the side feeder in the extrusion process. These averages were used to calculate the PP weight that should be added to each MB to prepare PP nanocomposites with 5 wt% Closite 15A. Table 3 shows that the amount of nanoclay in these samples is in the acceptable range.

Differential Scanning Calorimetry and Crystallinity. Differential scanning calorimetry was used to evaluate the thermal behavior of PP and PP/clay nanocomposite specimens and to estimate the percentage of crystalline phase in the samples. It has been reported that the clay particles act as nucleating agents for the crystallization of PP and that they cause an increase of PP crystallinity [25].

The percent crystallinity was determined as follows (*Eq. 4*):

$$\chi = \frac{\Delta H_{\mathrm{m}}}{f_{\mathrm{p}} \Delta H_{\mathrm{f}}^{o}}, \tag{4}$$

 DOI 10.1002/pen

TABLE 4. Percent of crystallinity and crystallization temperature.

Material name	Crystallinity (%)	Crystallization temperature
PP	34	112 (°C)
N1	41	130 (°C)
N2	42	132 (°C)
N3	41	117 (°C)
N4	44	118 (°C)

where ΔH_m (J/g) is the latent heat of fusion of the nanocomposite measured by DSC, f_p is the PP weight fraction in the nanocomposite, and Δ_f^o is the theoretical latent heat of fusion of a pure crystalline PP, namely 207 J/g [26]. Table 4 shows that crystallinity in the nanocomposite increased by about 10% compared to pure PP. On the other hand, the significant increase in crystallization temperature (~20°C) could be beneficial for molding applications, because of the faster solidification and shorter cycle time.

Clay Dispersion in PP and TPE Nanocomposite. X-ray diffraction analysis was performed on Cloisite 15A, PP nanocomposites, and TPE nanocomposites. Figure 2a shows the results for Cloisite 15A. There are three peaks in the range of 2° to 10°. The first peak is related to the basal spacing (d_{001}) of Cloisite 15A which appears at $2\theta = 2.85°$ (corresponding d-spacing is 3.1 nm). The second characteristic peak of the clay is observed as a shoulder in the vicinity of the first one at $2\theta = 4.6°$ (corresponding d-spacing is 1.9 nm) and the last peak for Cloisite 15A appears at $2\theta = 7.17°$ (corresponding d-spacing is 1.1 nm) which can be attributed to the portion of the clay that is not properly modified.

The results shown in Fig. 2 demonstrate that the degree of intercalation depends on the compatibilizer. The XRD pattern for N4 shows that the three peaks of Cloisite 15A (Fig. 2b), are shifted to lower angles corresponding to a change in d-spacing from 3.1 to 3.8 nm. The higher basal spacing of clay in comparison with the virgin Cloisite 15A suggests intercalation by the polymer chains.

The XRD patterns of N1, N2, and N3 nanocomposites show only two peaks in the range of 2° to 10° (Fig. 2c). The first observed peak at $2\theta \cong 2.64°$ corresponds to d-spacing of about 3.3 nm and the second peak is at $2\theta \cong 6.5°$. It is likely that these two peaks are related to the second and third peaks of Cloisite 15A at $2\theta \cong 4.6°$ and $2\theta \cong 7°$, respectively. All of the peaks of Cloisite 15A, with positions indicated by arrows in Fig. 2c, were shifted to lower angles. The first characteristic peak of Cloisite 15A, at $2\theta = 2.85°$, was shifted to angles below $2\theta \cong 2°$. However, because of the high intensity of the X-ray beam in this range, the detector could not detect this small portion of MMT layers.

To overcome the above problem and reduce the X-ray beam intensity in the range of $2\theta \cong 0.5°$ to 2°, a thin steel knife and cylindrical base were used as a sample holder to prevent edge effect. The setup adjusted in a manner that the upper surface of the sample touched the edge of the knife entirely. Also, great care was taken to

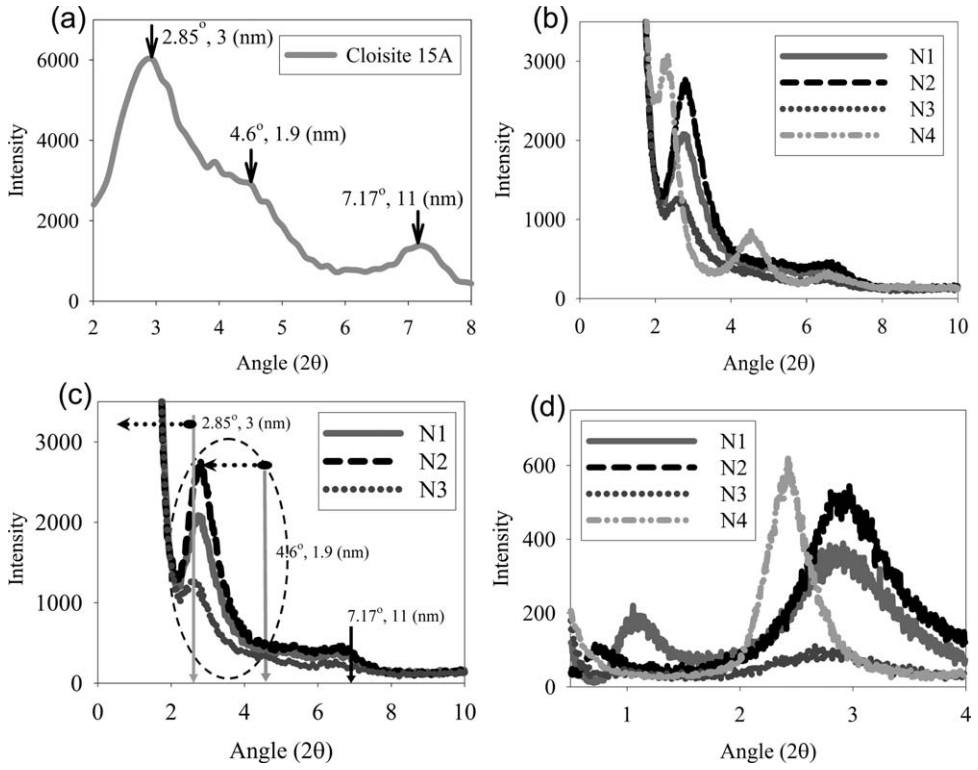

FIG. 2. XRD patterns of Cloisite 15A and nanocomposites at different scan range.

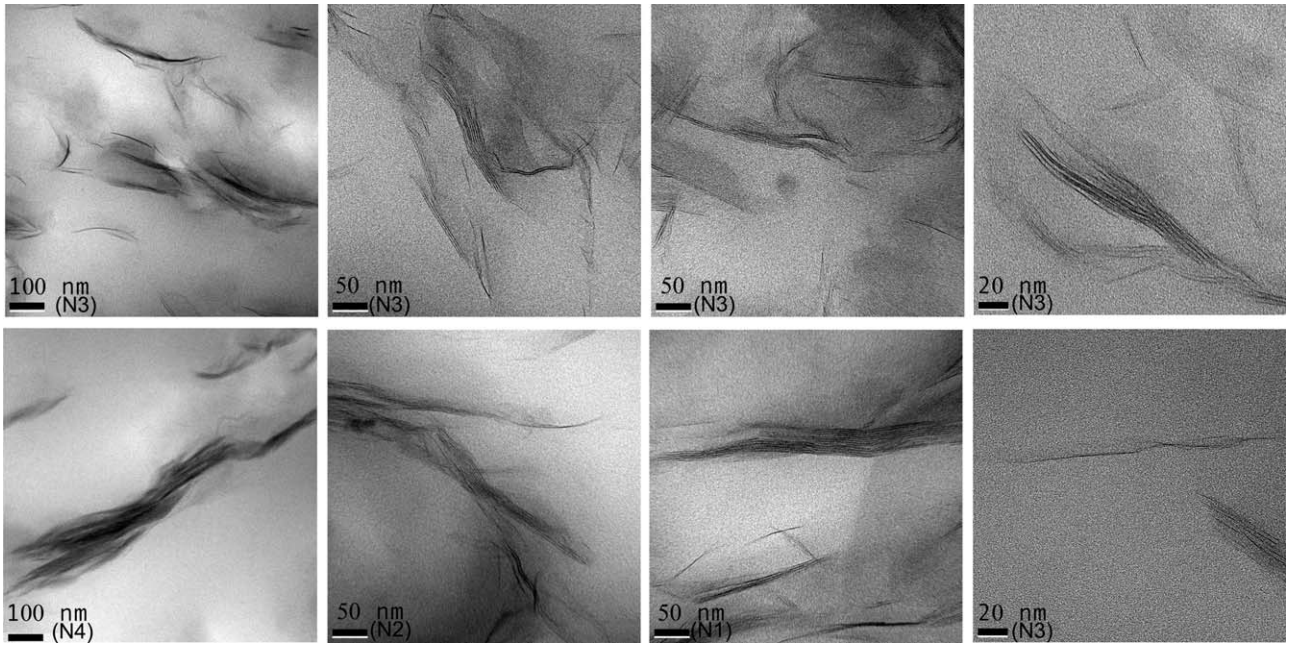

FIG. 3. TEM micrographs of PP nanocomposites.

align the edge of the knife with the X-ray generator and detector. This setup is a simplified model of the system used by Dell'Anno [26] to obtain data at smaller angles using the WAXD technique. After optimization of sample thickness, slit size, frame size, starting angle and scan rate to obtain reproducible data, X-ray scans were performed in the range of $2\theta = 0.5^\circ$ to $2\theta = 4^\circ$.

It is suggested that the peaks observed in Fig. 2d in the range of $2\theta = 0.5^\circ$ to $2\theta = 2^\circ$ are attributed to the intercalation of polymer chains in Cloisite 15A, into galleries with the original d-spacing of about 3.1 nm (at $2\theta \cong 2.8^\circ$). This peak is absent in pure PP and N4 nanocomposite. The above XRD analyses suggest a coexistence of intercalated MMT tactoids and exfoliated MMT layers in N1, N2, and N3 nanocomposites.

TEM images shown in Fig. 3 confirm the existence of intercalated dispersed tactoids containing small numbers of clay layers. These tactoids are well dispersed and separated from each other. The observed "semi-exfoliated" structure tends to confirm the XRD results.

The quality and uniformity of dispersion of nanoclay were investigated by SEM. The amorphous phase of PP was removed chemically from the microtomed surface. Thus, the nanoclays could be observed by SEM. Figure 4 shows that the agglomerates were uniformly dispersed in the matrix with no large particles, reflecting good mixing quality. Examination of micrographs at higher magnification suggested that nanoclay dispersion quality in N3 nanocomposite was better than that in N2 and N1. Tactoids observed in N2 and N1 were longer than those in N4, possibly due to slippage of MMT layers over each other, due to the higher intercalation of polymer chains.

According to the XRD analysis of TPEs (see Fig. 5), it seems that the higher shear stress, as a result of the incorporation of EPDM into the system, did not enhance polymer intercalation significantly.

The Correlation Between Rheological Behavior of PP-g-MA and Nanoclay Dispersion

Thermal Stability of PP-g-MA During Rheological Tests. To assess the thermal stability of the samples, a time sweep was carried out in the ARES device at 6.285 rad/s over 1 h at 200°C (processing temperature). Measurements were made under nitrogen atmosphere to reduce degradation risk. Table 5 shows the maximum changes in complex viscosity and storage modulus of the neat polymers. The change in the above properties of the compatibilizers was more pronounced than for PP and EPDM. This may be attributed to residual chemicals from MA grafting reaction. As all rheological measurements in this study were completed in <1 h, it is safe to assume that no degradation occurred during processing.

Determination of Linear Zones in Rheological Tests. To ensure that oscillatory shear measurements are conducted within the linear regime, stress sweep experiments were performed, using a parallel plate rheometer (ARES from Rheometrics Scientific) with parallel disc geometry of 25 mm diameter and 1.1 mm gap. Experiments were repeated at three frequencies. Theoretically, the stress limit at low frequency should also apply at high frequency. However, sometimes, as in the present case, this value is so small in the high frequency range that it limits

 DOI 10.1002/pen

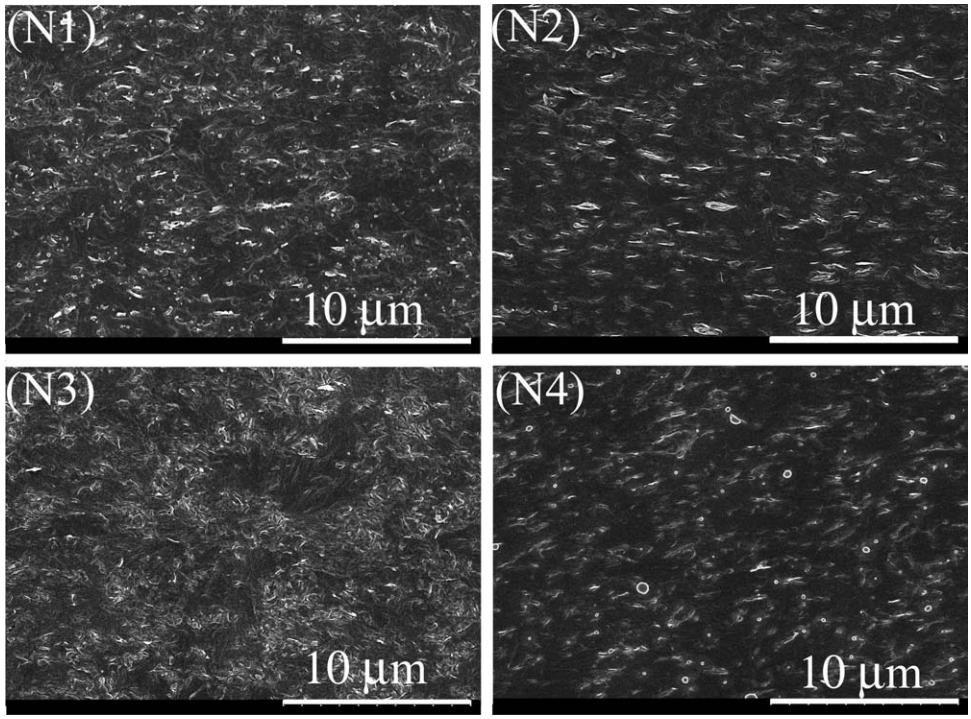

FIG. 4. SEM images of PP nanocomposites after removing the amorphous phase.

the precision of data. Therefore, frequency sweep experiments were carried out following several sequences, as shown in Table 6. In this way, both linearity and accuracy of measurement were taken into account.

Correlation Between Compatibilizer Viscosity and Clay Dispersion in TPEs. Dynamic measurements were performed using parallel plate geometry to determine material functions of the pure compatibilizers. At least four experiments were carried out for each material.

Figure 6 shows the complex viscosities of the four compatibilizers. It is clear that there is no evidence of a Newtonian-plateau at low frequencies. Within the experimental window employed, the complex viscosity of the compatibilizer with 35 MFI (No. 4) is higher than the complex viscosity of the compatibilizer with 10 MFI of (No. 3).

XRD analysis results shown in Fig. 2d indicated that sample N3 exhibits a coexistence of intercalated MMT tactoids and exfoliated MMT layers. Sample N4 exhibits mainly intercalated structure, while the dispersion levels in N1 and N2 nanocomposites are between those in N3 and N4. Sample N1 appears to have better platelet dispersion than N2, based on XRD, SEM, and TEM results (Figs. 3 and 4). Thus, it is possible to rank the dispersion quality in the nanocomposites in the following descending order: N3, N1, N2, and N4.

An attempt to find a correlation between complex viscosity and XRD patterns showed that as the compatibilizer viscosity decreased, the dispersion level first decreased, then it unexpectedly increased significantly.

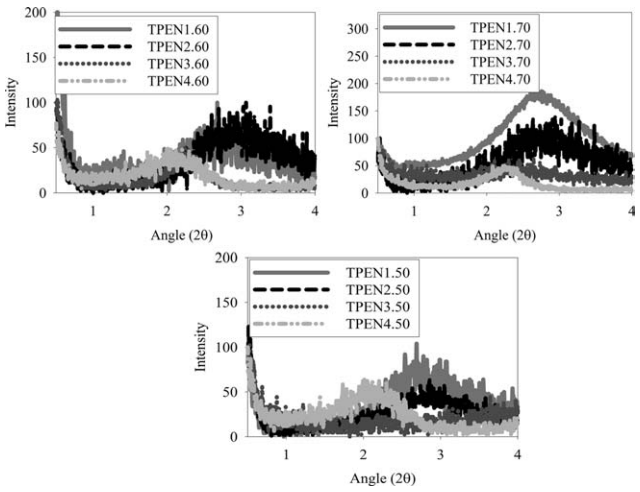

FIG. 5. XRD patterns of TPE nanocomposites at different EPDM content.

TABLE 5. Change in storage modulus and complex viscosity of neat materials after 1 h at 200°C.

Materials	Variation in storage modulus (%)	Variation in complex viscosity (%)
PP	5	4
EPDM	5	3
1	7	5
2	7	5
3	10	7
4	8	7

TABLE 6. Stress values at three sequences for frequency sweep tests.

Frequency (rad/s)	0.628–6.28	6.28–62.8	62.8–628
Stress (Pa) for compatibilizers	20	100	400
Stress (Pa) for nanocomposites	50	500	1000

Obviously, various factors, such as acid content (functionality), molecular weight, and processing conditions influence the contribution of the compatibilizer to dispersion and intercalation. It seems that complex viscosity behavior does not reflect the balance of the various contributions of these factors to the quality of dispersion. Therefore, another rheological parameter was sought that might show better correlation with XRD observations.

Correlation Between Compatibilizer Relaxation Time and Clay Dispersion in TPEs. The characteristic relaxation time of each compatibilizer was calculated, using the corresponding storage and loss moduli obtained in frequency sweep experiments. The results are shown in Table 7.

Moreover, stress relaxation experiments were carried out using an applied strain of 0.2 at 200°C. Figure 7 shows the normalized stress relaxation moduli of the pure compatibilizers versus time. Table 7 and Fig. 7 indicate that there is a direct relation between relaxation time and polymer chain intercalation in nanoclays. As the relaxation time of the compatibilizer increases, the extent of intercalation in the corresponding nanocomposite becomes higher.

It is suggested that, during the mixing process in the twin screw extruder, compatibilizer chains enter the narrow interlayer galleries of the nanoclays. When shearing stops, as the melt leaves the die, compatibilizer chains tend to recover their entropies by diffusing out and recoiling in the vicinity of MMT layers, because of the favorable interaction between MA groups and MMT layers. If the relaxation time of the compatibilizer is higher, the recoiling and diffusion process requires longer time. This permits the PP chains to enter the enlarged galleries and to form intercalated structures. This seems to explain the good correlation between higher relaxation time of the compatibilizer and the degree of intercalation in the nanocomposite.

TABLE 7. Characteristic relaxation time at 200°C, $\omega = 1$ Hz.

Compatibilizer	G'	G''	$\lambda = G'/(G''\omega)$
1	8304	13,200	0.62
2	4671	8999	0.51
3	748	1011	0.73
4	1174	2592	0.45

The Effect of Nanoclay Dispersion Level on Co-Continuity and Morphology of TPEs

The Rubber Phase Continuity in TPEs. Interfacial tension, viscosity ratio, and processing conditions influence the continuity index. The interfacial tension between PP and EPDM is very low (~0.3 mN/m at 190°C) [27]. A system with such low interfacial tension should exhibit very broad regions of co-continuity [16]. Figure 8 shows that the differences among the nanocomposite viscosities at high frequencies were not large.

A single master-curve for continuity development was observed for the TPE blends at viscosity ratios between 0.7 and 5.0. This would suggest that the observed differences in the continuity index (Fig. 9a) could not be the result of different viscosity ratios of the thermoplastic and rubber phases. As the processing conditions used in nanocomposite preparation were the same, the observed differences in continuity index might be attributed to the presence of clay in the system. Figure 9a shows that the incorporation of clay causes a reduction of the continuity

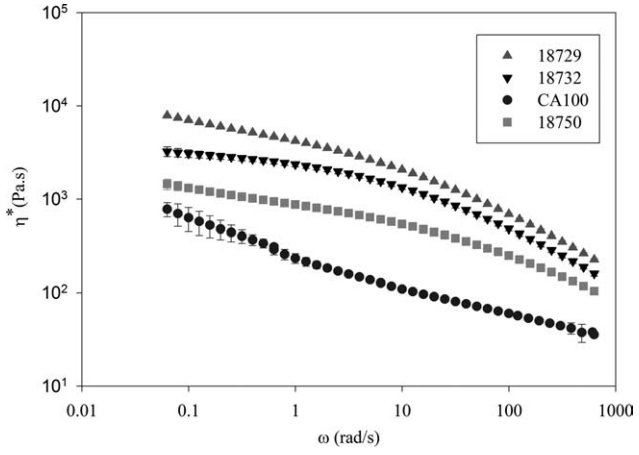

FIG. 6. Complex viscosity as a function of angular frequency for pure compatibilizers.

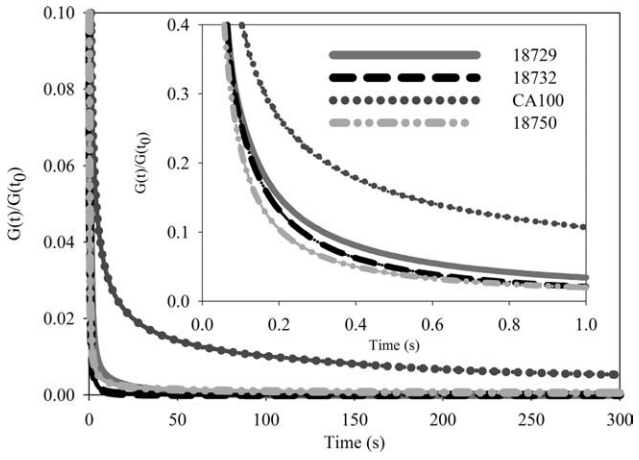

FIG. 7. Normalized stress relaxation modulus as a function of time for pure compatibilizers at 200°C.

DOI 10.1002/pen

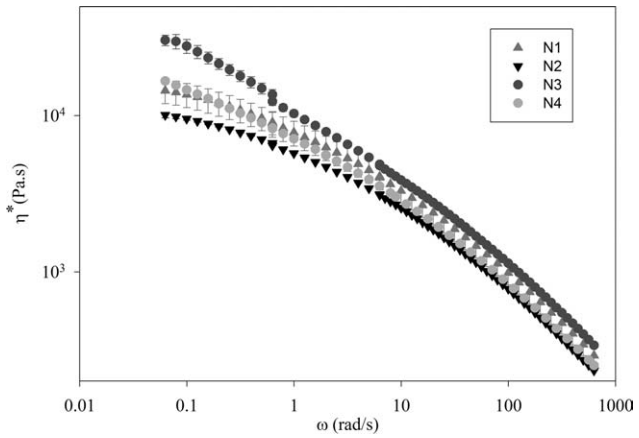

FIG. 8. Complex viscosity as a function of angular frequency for PP nanocomposites.

index of the EPDM phase. The effect is more pronounced in the intercalated nanocomposites than in the semi-exfoliated nanocomposites.

Figure 10 shows micrographs of the EPDM phase in intercalated and semi-exfoliated nanocomposites, at 50 wt% EPDM. These images clearly point to the higher connectivity of the EPDM phase in the TPEs prepared using "intercalated/exfoliated" PP nanocomposites as the thermoplastic phase.

The above differences in the blend morphology influence the rheological behavior of TPE nanocomposites at the specified composition. It was found that stress growth viscosity is more sensitive to the continuity index than other material functions obtained using frequency sweep, stress relaxation, and creep experiments. The physical significance of the stress overshoot is that it indicates impending structural change [28]. Figure 11a reveals that a higher EPDM continuity index is associated with a lower overshoot of normalized stress growth viscosity, in cases where PP was the continuous phase.

Polymers that adapt themselves to stress can damp the applied stress or sustain uniform shear, and thus the overshoot would not be observed. When PP is the continuous phase, the stress is transferred to the EPDM phase. Because deformation of the isolated domains of EPDM would be easier than alteration of the coherent continuous structure permeating the whole volume, a higher EPDM continuity index leads to a lower overshoot of normalized stress growth viscosity (Fig. 11a). Thus, it is likely that the rubber phase could adapt itself to the applied stress more readily, when the rubber connectivity is more complete. These observations are potentially useful to provide qualitative information about continuity indices, especially in view of the time consuming solvent extraction and gravimetry measurements.

Thermoplastic Phase Continuity. Since, most PP solvents would also dissolve EPDM, it is difficult to determine PP continuity by solvent gravimetry. To overcome this difficulty the irradiation crosslinking method was used. Upon gamma irradiation, by beta decay of $_{27}$Co, high local concentrations of free radicals are formed in the rubber molecules. The crosslinking mechanism is similar to that obtained with peroxide crosslinking. Homogeneous crosslinking can be achieved, because of the tissue penetrating property of gamma rays [24]. A dose rate of 20 kGy/h and a total dose of 160 kGy were used to prevent the chain scission reaction. The gel content of irradiated pure EPDM was estimated with the same procedure used for PP dissolution. Because of the chain scission of EPDM to a certain extent by gamma irradiation and the presence of noncrosslinkable EPDM, the difference between the weight of the sample before and after extraction is related to the continuous portion of PP in the blend with the addition of small fraction of EPDM that should be subtracted. In the present case, the solubility of irradiated EPDM was found to be about 3.5 wt% in boiling xylene and corrections were applied appropriately to the PP continuity development curve.

Figure 9b shows continuity development of the thermoplastic phase for each nanocomposite. It is clear that an increase in the EPDM content leads to a reduction of the continuity index of the thermoplastic phase. However,

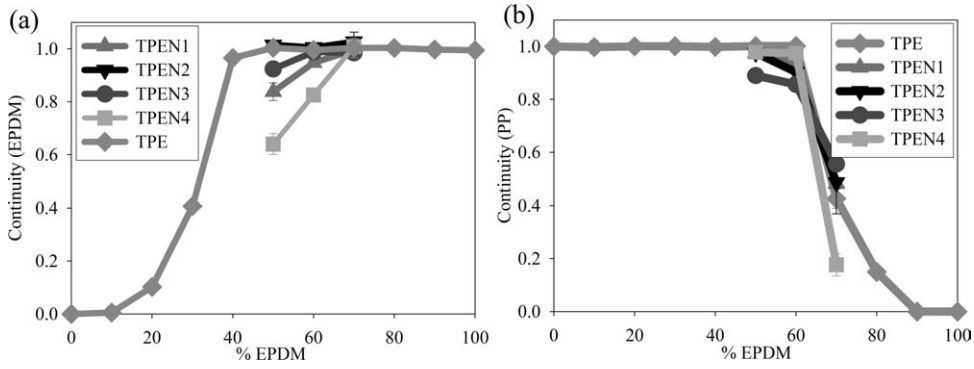

FIG. 9. The continuity indices of EPDM (a) from noncrosslinked specimens and PP (b) from irradiated samples (corrected for thermoplastic phases solubility in cyclohexane at room temperature, and irradiated EPDM solubility in xylene).

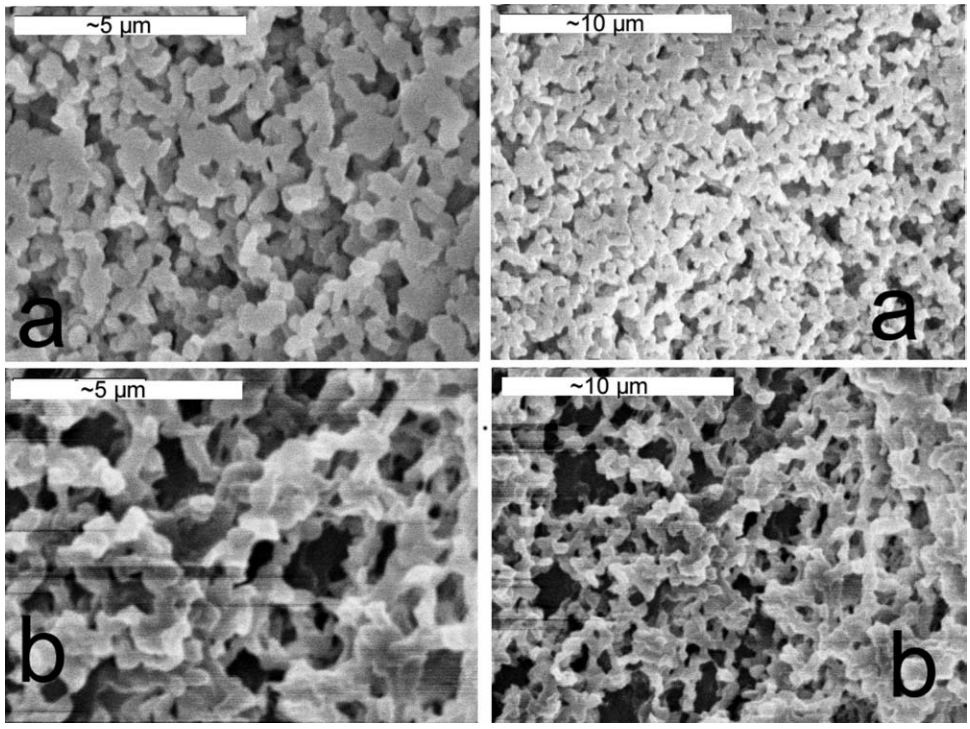

FIG. 10. SEM micrographs of TPE nanocomposites after partial PP matrix dissolution. (a) Exfoliated system TPEN3.50, (b) intercalated system TPEN4.50.

the rate of reduction decreases when the dispersion level improves. Although intercalation leads to the low continuity of the thermoplastic phase, the continuity index of TPEN3.70 prepared using the semi-exfoliated PP nanocomposite is about 0.2 higher than that of TPE prepared using pure PP. As $Ca \gg 1$ for this system, the mixing process involves basically distributive mixing that leads to rearrangement and deformation of the phases. The main break-up mechanism is due to the breakup of highly elongated threads via capillary instabilities that produce a line of smaller droplets. Breakup occurs when a thread diameter for which $Ca < 1$ is reached, if the residence time during the mixing process is longer than their break-up time. Thus, the higher continuity of PP in semi-exfoliated systems may be attributed to the higher melt strength of the thermoplastic threads of semi-exfoliated system. Larger tactoids act as defects that reduce break-up times. Figure 12 shows SEM images of TPEs based on intercalated and semi-exfoliated systems at 70% of EPDM.

The thermoplastic phase droplets in the semi-exfoliated system are smaller and more elongated than droplets in intercalated TPEs. Although it is difficult to infer the real TPE morphology using two-dimensional images, D_n and D_v, the number and volume average diameters, respec-

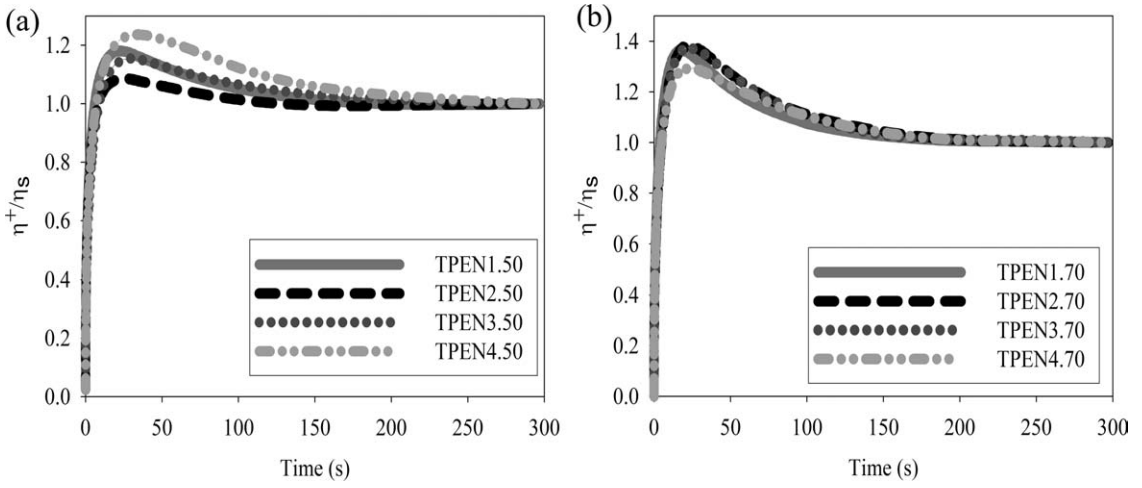

FIG. 11. Normalized stress growth viscosity as a function of time for (a) TPENx.50 and (b) TPENx.70.

 DOI 10.1002/pen

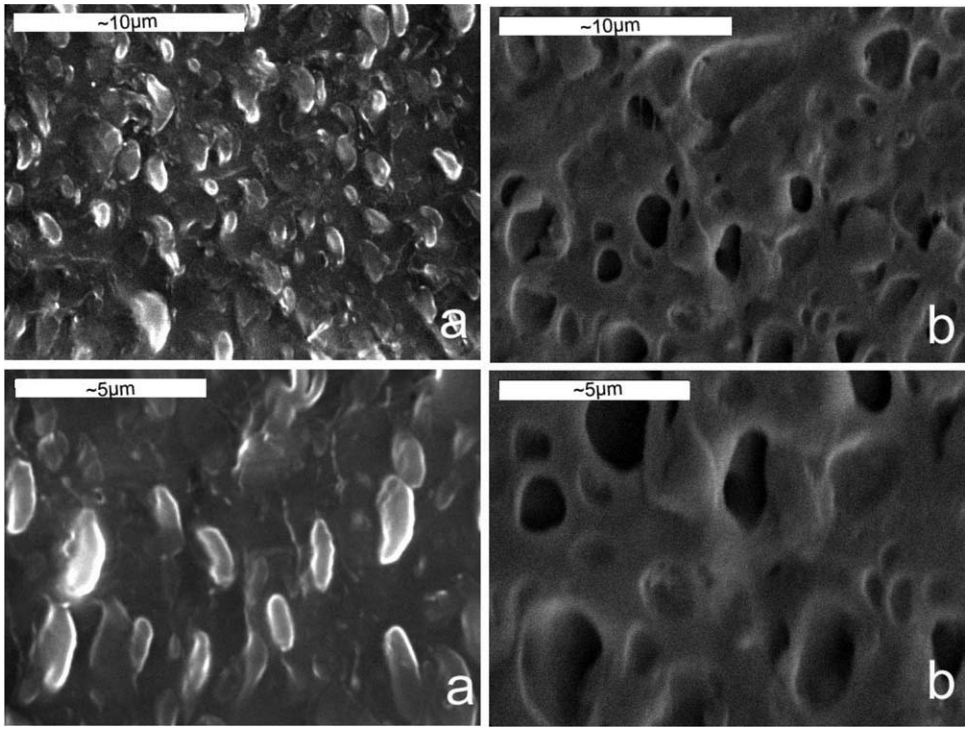

FIG. 12. Micrographs of TPE nanocomposites after PP dissolution for (a) semiexfoliated system TPEN1.70, (b) intercalated system TPEN4.70.

tively, for the semi-exfoliated system were calculated 1.3 and 1.6 μm, respectively in comparison with D_n of 1.6 μm and D_v of 1.8 μm for the intercalated system. At high EPDM composition, it was found again that the significant change in morphology could influence the overshoot of normalized stress growth viscosity. Here, because the

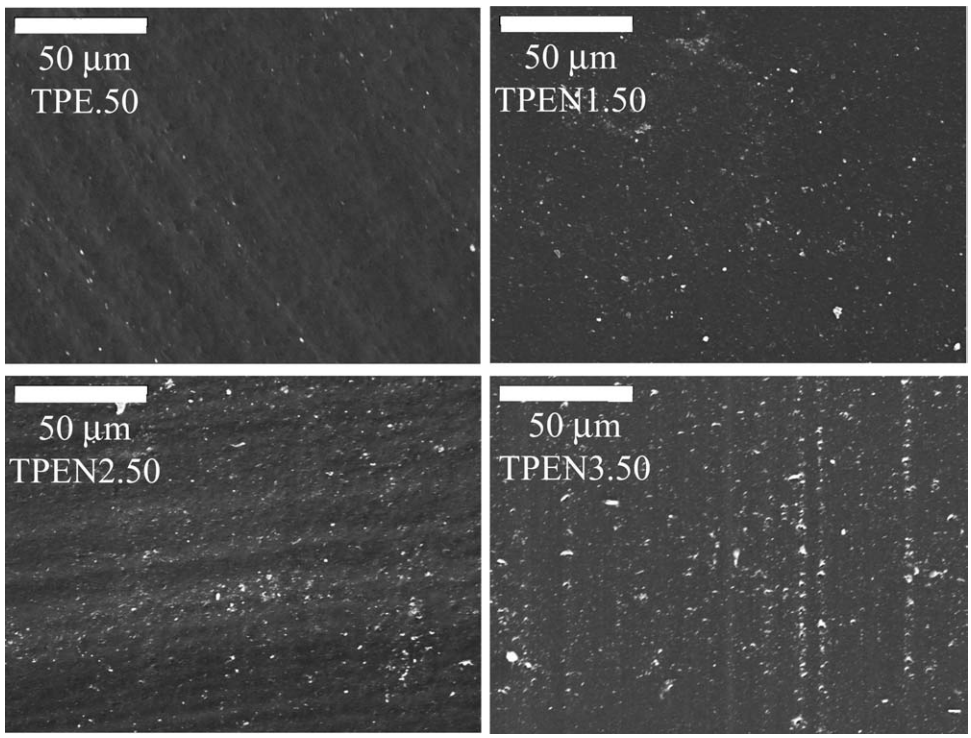

FIG. 13. Micrographs of irradiated TPE nanocomposites after complete PP dissolution (bright spots show accumulated nanoclay agglomerates).

higher viscosity component is the matrix, when the continuity of the thermoplastic phase decreases, the amount of overshoot decreases (Fig. 11b).

It should be mentioned that there are some evidences that clay remained mainly in the PP phase. After complete extraction of thermoplastic phase, the clay particles could be observed clearly on the wall of the thimbles. However, there was no trace of clay powder in the solution or on the wall of centrifuge tube that were used to complete extraction of EPDM phase. Moreover, Fig. 13 shows accumulated nanoclay agglomerates in the irradiated samples after complete thermoplastic phase dissolution (bright spots). These big agglomerates formed in the free domains that had been filled by the thermoplastic phase before PP dissolution. These bright spots were not detected in the bulk, when EPDM was extracted completely. Therefore, it may be concluded that the nanoclay remained in the thermoplastic phase. This is in agreement with reported observations that nanoclay remains mainly in the low viscosity phase or the phase which the clay was originally incorporated in [18, 29].

CONCLUSIONS

The effects of compatibilizer on the nanoclay dispersion level and co-continuity in TPE nanocomposites were investigated. The relaxation behavior of compatibilizer was found to correlate with the extent of intercalation and nanoclay dispersion. Higher relaxation times of the compatibilizer were associated with better dispersion of nanoclay.

It was also found that the presence of nanoclay reduces the co-continuity composition range. However, better dispersion of the nanoclay limits the reduction of the thermoplastic phase continuity.

The present study suggests that the optimization of the microstructure and properties of TPV/clay nanocomposites is enhanced by the optimization of the microstructure of their precursor TPE/clay nanocomposites.

ACKNOWLEDGMENT

The authors thank Prof. Monique Lacroix and Guy Desroches of the INRS-Institut Armand-Frappier, Université du Québec for irradiating the blends.

REFERENCES

1. M. Avella, S. Cosco, G. della Volpe, and M.E. Errico, *Adv. Polym. Technol.*, **24**(**2**), 132 (2005).
2. K.Y. Lee and L.A. Goettler, *Polym. Eng. Sci.*, **44**(**6**), 1103 (2004).
3. M. Kawasumi, N. Hasegawa, M. Kato, A. Usuki, and A. Okada, *Macromolecules*, **30**(**20**), 6333 (1997).
4. W. Lertwimolnun and B. Vergnes, *Polymer*, **46**(**10**), 3462 (2005).
5. S. Hambir, N. Bulakh, and J.P. Jog, *Polym. Eng. Sci.*, **42**(**9**), 1800 (2002).
6. P. Reichert, H. Nitz, S. Klinke, R. Brandsch, R. Thomann, and R. Mülhaupt, *Macromol. Materials Eng.*, **275**(**1**), 8 (2000).
7. M. Kato, A. Usuki, and A. Okada, *J. Appl. Polym. Sci.*, **66**(**9**), 1781 (1997).
8. N. Hasegawa, M. Kawasumi, M. Kato, A. Usuki, and A. Okada, *J. Appl. Polym. Sci.*, **67**(**1**), 87 (1998).
9. P. Svoboda, C. Zeng, H. Wang, L.J. Lee, and D.L. Tomasko, *J. Appl. Polym. Sci.*, **85**(**7**), 1562 (2002).
10. M. Ton-That, F. Perrin-Sarazin, K.C. Cole, M.N. Bureau, and J. Denault, *Polym. Eng. Sci.*, **44**(**7**), 1212 (2004).
11. P. Potschke and D.R. Paul, *Polym. Rev.*, **43**(**1**), 87 (2003).
12. J. Lyngaae-Jorgensen, K. Lunde Rasmussen, E.A. Chtcherbakova, and L.A. Utracki, *Polym. Eng. Sci.*, **39**(**6**), 1060 (1999).
13. N. Mekhilef, B.D. Favis, and P.J. Carreau, *J. Polym. Sci. B Polym. Phys.*, **35**(**2**), 293 (1997).
14. J. He, W. Bu, and J. Zeng, *Polymer*, **38**(**26**), 6347 (1997).
15. J. Lyngaae-Jorgensen, A. Kuta, K. Sondergaard, and K.V. Poulsen, *Polym. Networks Blends*, **3**(**1**), 1 (1993).
16. P. Bhadane, M. Champagne, M. Huneault, F. Tofan, and B. Favis, *Polymer*, **47**(**8**), 2760 (2006).
17. R.C. Willemse, A.P. de Boer, J. van Dam, and A.D. Gotsis, *Polymer*, **39**(**24**), 5879 (1998).
18. G. Naderi, P.G. Lafleur, and C. Dubois, *Int. Polym. Process.*, **3**, 284 (2007).
19. D. Hoon Kim, P.D. Fasulo, W.R. Rodgers, and D.R. Paul, *Polymer*, **48**(**20**), 5960 (2007).
20. H.-S. Lee, P.D. Fasulo, W.R. Rodgers, and D.R. Paul, *Polymer*, **46**(**25**), 11673 (2005).
21. D.H. Kim, P.D. Fasulo, W.R. Rodgers, and D.R. Paul, *Polymer*, **49**(**10**), 2492 (2008).
22. B.D. Favis and J.P. Chalifoux, *Polym. Eng. Sci.*, **27**(**21**), 1591 (1987).
23. J. Park, K. Eom, O. Kwon, and S. Woo, *Microscopy Microanal.*, **7**, 276 (2001).
24. T. Özdemir, *Radiation Phys. Chem.*, **77**(**3**), 787 (2008).
25. A. Pozsgay, T. Frater, L. Papp, I. Sajo, and B. Pukanszky, *J. Macromol. Sci. B*, **41**(**4**), 1249 (2002).
26. G. Dell'Anno, "Development of a New Class of Hybrid Reinforced Thermoplastic Composites Based on Nanoclays and Woven Glass Fibers," Ph.D. Thesis, University of Pisa, Italy (2004).
27. A.Y. Coran, R.P. Patel, and S. William, *Rubber Chem. Technol.*, **55**(**1**), 116 (1981).
28. R. Sham and W. Shi-Qing, *J. Rheol.*, **52**(**3**), 681 (2008).
29. H. Thakkar, K.Y. Lee, and L.A. Goettler, "Phase Reinforcement Effects in TPV Nanocomposites," in *SPEANTEC Proceedings*, Nashville, TN, **61**, 3009 (2003).